

Primordial Black Holes as Dark Matter: Constraints From Compact Ultra-Faint Dwarfs

Qirong Zhu^{1,2*}, Eugene Vasiliev^{3,4}, Yuexing Li^{1,5}, and Yipeng Jing⁵

¹*Department of Astronomy & Astrophysics; Institute for Cosmology and Gravity, The Pennsylvania State University, PA 16802, USA*

²*Harvard-Smithsonian Center for Astrophysics, Harvard University, 60 Garden Street, Cambridge, MA 02138, USA*

³*Rudolf Peierls Centre for Theoretical Physics, 1 Keble road, Oxford, UK, OX1 3NP*

⁴*Lebedev Physical Institute, Leninsky prospekt 53, Moscow, Russia, 119991*

⁵*Tsung-Dao Lee Institute; Department of Astronomy, Shanghai Jiao Tong University, 800 Dongchuan Road, Shanghai 200240, China*

Accepted XXX. Received YYY; in original form ZZZ

ABSTRACT

The ground-breaking detections of gravitational waves from black hole mergers by LIGO have rekindled interest in primordial black holes (PBHs) and the possibility of dark matter being composed of PBHs. It has been suggested that PBHs of tens of solar masses could serve as dark matter candidates. Recent analytical studies demonstrated that compact ultra-faint dwarf galaxies can serve as a sensitive test for the PBH dark matter hypothesis, since stars in such a halo-dominated system would be heated by the more massive PBHs, their present-day distribution can provide strong constraints on PBH mass. In this study, we further explore this scenario with more detailed calculations, using a combination of dynamical simulations and Bayesian inference methods. The joint evolution of stars and PBH dark matter is followed with a Fokker–Planck code PHASEFLOW. We run a large suite of such simulations for different dark matter parameters, then use a Markov Chain Monte Carlo approach to constrain the PBH properties with observations of ultra-faint galaxies. We find that two-body relaxation between the stars and PBH drives up the stellar core size, and increases the central stellar velocity dispersion. Using the observed half-light radius and velocity dispersion of stars in the compact ultra-faint dwarf galaxies as joint constraints, we infer that these dwarfs may have a cored dark matter halo with the central density in the range of 1–2 M_{\odot}/pc^3 , and that the PBHs may have a mass range of 2–14 M_{\odot} if they constitute all or a substantial fraction of the dark matter.

Key words: cosmology:dark matter – galaxies: dwarfs – methods: numerical

1 INTRODUCTION

In the standard Lambda cold dark matter (Λ CDM) cosmology, the nature of the DM remains elusive. The possibility of DM being composed of primordial black holes (PBHs, [Hawking 1971](#)), arising naturally from certain inflation models (e.g., [Frampton et al. 2010](#)), has been investigated in the context of galaxy formation early on (e.g., [Carr & Hawking 1974](#); [Mészáros 1975](#)), and it has not yet been completely ruled out (see recent reviews by [Carr et al. 2016](#)). Recently, it was suggested that three mass windows, around $5 \times 10^{-16} M_{\odot}$, $2 \times 10^{-14} M_{\odot}$ and 25–100 M_{\odot} , respectively, are still open for DM consists of PBHs ([Carr et al. 2017](#)).

The recent detections of gravitational waves by LIGO are believed to originate from merging black holes with

masses of order 10–50 M_{\odot} , significantly higher than known BHs in Galactic X-ray binaries ([The LIGO Scientific Collaboration et al. 2016a,b, 2017b,a](#)). These discoveries have renewed theoretical interest in PBHs as a DM candidate. It was suggested by [Bird et al. \(2016\)](#) that PBHs with a mass around 30 M_{\odot} are loosely constrained by micro-lensing experiments and that the merger rate of binary PBHs is consistent with the LIGO detections.

If true, PBHs in this mass range could be an attractive DM candidate to solve some well-known problems on the galactic scale (see [Weinberg et al. 2015](#)), in particular the “cusp vs. core problem” (hereafter, we refer to dark matter made of primordial black holes as PBH-DM). The PBHs would produce DM cores instead of cusps in the central galaxy because any “temperature inversion” present in a cuspy profile will lead to a removal the density cusp by increasing the velocity dispersion ([Quinlan 1996](#)). Solutions

* E-mail: qxz125@psu.edu

to the “cusp vs. core problem” based on baryonic heating of DM are shown to be mass-dependent (Pontzen & Governato 2014; Di Cintio et al. 2014; Chan et al. 2015). The survival of a globular cluster in the ultra-faint dwarf galaxy Eridanus II, however, hints to a DM core in a galaxy halo where any baryonic effect would be weak (Amorisco 2017; Contenta et al. 2017).

In addition, a cosmology model with PBHs as DM indicates a rather different evolution picture from that of other types of DM, such as *warm dark matter*, *fuzzy dark matter* (Hu et al. 2000; Hui et al. 2017), and *self-interacting dark matter* (Vogelsberger et al. 2012). Contrary to a common feature of suppressed small-scale perturbations in these models (Vogelsberger et al. 2016), fluctuations in the number density of PBH impose *additional* small-scale power (Afshordi et al. 2003). As a result, low-mass PBH-DM halos will form ahead of Λ CDM halos, while in *warm/fuzzy dark matter*, the DM halo formation is considerably delayed, which has a strong consequence on the onset of reionization (Yoshida et al. 2003; Hirano et al. 2017).

Despite these appealing features, it remains unclear what fraction of the DM can PBHs constitute, and what mass range can these PBHs have. Fortunately, a population of compact (with projected half-light radius of ~ 30 pc), ultra-faint ($\sim 1000 L_{\odot}$) dwarf galaxies has recently been discovered (e.g. Koposov et al. 2015; Bechtol et al. 2015), and they are expected to provide stringent constraints on the PBH-DM. Using analytical approaches, Brandt (2016) suggested that two-body relaxation between stars and PBH-DM would drive a substantial size evolution in galaxies, which is inconsistent with the observed small size of the ultra-faint dwarfs, while Koushiappas & Loeb (2017) argued that mass segregation would rearrange the stars into an otherwise detectable ring in the surface brightness profile of Segue I.

In order to improve these analytical studies, we combine two methods, Fokker–Planck (FP) simulations and Markov Chain Monte Carlo (MCMC) modeling, to study the evolution of galaxy halos containing both stars and PBH-DM and to compare with observations. We first use an FP code to perform a large set of galaxy simulations with different parameters for the PBH-DM to follow the interaction and evolution of the stars and PBHs, then we employ an MCMC method to constrain the PBH properties using the observed half-light radius and velocity dispersion of stars in compact ultra-faint galaxies. Our modeling presents a significant improvement over the previous studies based on an analytical form of energy diffusion coefficient and other simplifying assumptions (Brandt 2016; Koushiappas & Loeb 2017).

This paper is organized as follows. In § 2, we describe the numerical code and MCMC algorithm used in our simulations and analysis. In § 3, we present the dynamical evolution of the stars and PBHs in the halo systems, and constraints from observations. We discuss the implications of our study and its limitations in § 4, and summarize our main findings in § 5.

2 METHODS

2.1 Numerical code for dynamical simulations

In this study, we use an FP code, PHASEFLOW¹ (Vasiliev 2017) to follow the dynamical evolution of stars and PBH-DM in the galaxy halos. PHASEFLOW solves the one-dimensional FP equation for the distribution function in energy, using a high-accuracy finite element method. The code is well tested with problems such as core collapse and the formation of Bahcall-Wolf cusp around a central massive black hole. PHASEFLOW can handle multiple mass components, which enables our calculations of the evolution of a halo of stars and DM consisting of PBHs. Once the initial conditions of the two components are specified, PHASEFLOW evolves the distribution function of all components while at the same time updating the gravitational potential. System diagnosis such as density profile and velocity dispersions are computed automatically, which greatly simplifies our analysis. Throughout the paper, we set the Coulomb logarithm (Binney & Tremaine 2008) $\ln \Lambda$ to be 15.

The stars in the DM halo are modeled with a Plummer sphere (Plummer 1911):

$$\rho(r) = \frac{3M_*}{4\pi R_{0,*}^3} \left(1 + \frac{r^2}{R_{0,*}^2}\right)^{-5/2}, \quad (1)$$

where the stellar system is characterized by the total stellar mass M_* and its scale radius $R_{0,*}$, respectively. In this calculation, we set $M_* = 10^3 M_{\odot}$, and each star particle has an equal mass of $1 M_{\odot}$.

The extended PBH-DM halo follows a Dehnen sphere (Dehnen 1993):

$$\rho(r) = \frac{(3-\gamma)M_{\text{DM}}}{4\pi R_{0,\text{DM}}^3} \left(\frac{r}{R_{0,\text{DM}}}\right)^{-\gamma} \left(1 + \frac{r}{R_{0,\text{DM}}}\right)^{\gamma-4}, \quad (2)$$

where M_{DM} is the total mass and $R_{0,\text{DM}}$ the scale radius of the halo, respectively. We choose the Dehnen sphere since it has finite mass in contrast to an Navarro-Frenk-White (NFW) profile (Navarro et al. 1997), while at the same time offers more flexibility than a Hernquist distribution (Hernquist 1990) or a truncated NFW profile. Note that the Dehnen sphere is a special case of the more general α - β - γ density profile (Zhao 1996), where the density distribution is determined by the inner slope γ and the outer slope β and the steepness parameter α , which control how quickly the inner slope transits into the outer slope.

2.2 Markov Chain Monte Carlo for parameter constraints

2.2.1 Observational data and the likelihood function

The MCMC is an effective method to explore multiple key parameters in a complex system. In our model, we use both the stellar half-light radius and the stellar velocity dispersion of the compact ultra-faint dwarfs to constrain the parameter space, which requires $\sim 10^5$ MCMC realizations. Fortunately, PHASEFLOW is an extremely efficient code, and it takes only

¹ PHASEFLOW is part of the AGAMA library for galaxy modeling, available from <https://github.com/GalacticDynamics-Oxford/Agama/>.

Table 1. A sample of observed compact ultra-faint dwarf galaxies used in our modeling from [Brandt \(2016\)](#).

Galaxy Name	Projected r_h [pc]	σ_* [km/s]	L_V [L_\odot]
Wil I	25 ± 6	$4.3^{+2.3}_{-1.3}$	1000
Seg I	29^{+8}_{-5}	$3.9^{+0.8}_{-0.8}$	300
Seg II	35 ± 3	$3.4^{+2.5}_{-1.2}$	900
Ret II	32^{+2}_{-1}	$3.2^{+1.6}_{-0.5}$	1500
Hor I	25^{+9}_{-4}	$4.9^{+2.8}_{-0.9}$	2000

several seconds to run a single model. Thus, we combine a large grid of FP simulations performed using PHASEFLOW and MCMC calculations using the EMCEE code. The EMCEE code uses an affine-invariant ensemble sampler to efficiently random walk the parameter space ([Foreman-Mackey et al. 2013](#)).

The likelihood function of our modeling is described in the following form:

$$\mathcal{L} = \prod_{i=1}^N \mathcal{N}(r_{h,M}, r_{h,O}, \epsilon_{h,O}) \mathcal{N}(\sigma_M, \sigma_O, \epsilon_{\sigma,O}), \quad (3)$$

where \mathcal{N} is a normal distribution, N is the sample size, $r_{h,M}$ is the model output of 3D half-mass radius, $r_{h,O}$ and σ_O are the observed half-light radius and velocity dispersion, respectively. The associated uncertainties are $\epsilon_{h,O}$ and $\epsilon_{\sigma,O}$.

We use the top five ultra-faint dwarf galaxies compiled by [Brandt \(2016\)](#) which have measurements of both size and stellar velocity dispersion available. The data is repeated here in Table 1 for convenience but we refer the readers to [Brandt \(2016\)](#) for details and references of each measurement. Note that there are discrepancies in the reported half-mass radius of the two newly discovered Ret II and Hor I between [Koposov et al. \(2015\)](#) and [Bechtol et al. \(2015\)](#). In each case, we have chosen the smaller value of the two measurements. The reason for such a sample is based on the implicit assumption (inherited from [Brandt \(2016\)](#)) that these five galaxies form a distinct class of faint dwarfs with similar size and velocity dispersion, which can be compared to a *single* theoretical model. Lastly, we apply a factor of 1.3 to de-project the observed half-mass radius to 3D following [Wolf et al. \(2010\)](#).

2.2.2 Selections of prior distributions

Total dark matter mass M_{DM}

Compact ultra-faint dwarf galaxies from our sample have the least amount of stars ($\sim 1000 L_\odot$) ever known, but their total mass remains unknown. It was suggested that they may reside in the least massive halos where atomic cooling is efficient, and that their total mass is around $10^9 M_\odot$ ([Sawala et al. 2015](#); [Wheeler et al. 2015](#); [Zhu et al. 2016](#)), since such a halo mass is consistent with the M_* – M_{DM} relations at the low mass end ([Garrison-Kimmel et al. 2017](#)). Recently, [Ma et al. \(2017\)](#) resolved the formation of such galaxies in their simulations, and reported that the least massive halo, which has a mass of $10^8 M_\odot$ at $z = 5$, had already stopped star formation since $z = 8$. On the other hand, [Read et al.](#)

(2016) modeled isolated dwarf galaxies and found that halos with a total mass of $10^8 M_\odot$ were able to match several dwarf satellites of the Milky Way.

Therefore, we choose a weakly informative prior of M_{DM} , which follows a log-normal distribution:

$$\log(M_{DM}) \sim \mathcal{N}(9, 0.5). \quad (4)$$

The choice of this prior is well justified in that the physics involved is relatively straightforward. These low-mass galaxies must be just massive enough, above the thresholds set by atomic cooling and UV background radiation, for stars to form (e.g., [Okamoto et al. 2008](#); [Gnedin & Kaurov 2014](#)). The width of the distribution also ensures that halos down to $2\text{--}3 \times 10^8 M_\odot$ are covered.

DM scale radius $R_{0,DM}$

From the discussion below (§ 3.1), we argue that the inner density profile of the halo will form a core ($\gamma = 0$) due to relaxation effect. However, the size of the scale radius needs to be treated as another free parameter in our model. This is largely due to a lack of self-consistent collisional N-body simulations from cosmological initial conditions. The assumption that the characteristic scales of the PBH-DM halos are similar to the Λ CDM models could lead to serious systematics. Thus, we adopt a log-uniform distribution of $R_{*,DM}$ for the range from 100 pc to 2000 pc:

$$\log(R_{*,DM}) \sim \mathcal{U}(\log(100), \log(2000)). \quad (5)$$

Stellar scale radius $R_{0,*}$

The heating of stars due to two-body relaxation increases the scale radius of stellar distribution roughly as $R_* \sim t^{0.5}$ ([Brandt 2016](#)), which indicates that the present-day size does not depend sensitively on the initial value of $R_{0,*}$. We thus use a log-uniform distribution for $R_{0,*}$ for the range from 10 pc to 50 pc.

$$\log(R_{0,*}) \sim \mathcal{U}(\log(10), \log(50)). \quad (6)$$

The lower limit corresponds to the largest Galactic globular clusters and the upper limit corresponds to the average size of the currently observed compact ultra-faint dwarfs.

Primordial BH mass M_{BH}

Lastly, the mass of the PBHs is not well constrained ([Carr et al. 2017](#)). PBHs above $100 M_\odot$ can be ruled out by CMB observation and the Galactic wide binaries (see [Carr et al. 2016](#)). However, since we are most interested in the range of $[1, 100] M_\odot$, we assume a log-uniformly distribution for M_{BH} in this range.

3 RESULTS

3.1 Cusp to core transition in PBH-DM halos from relaxation effect

In a CDM halo, the density profile usually shows a central density cusp with a slope in the range of $0 < \gamma < 2$, and the

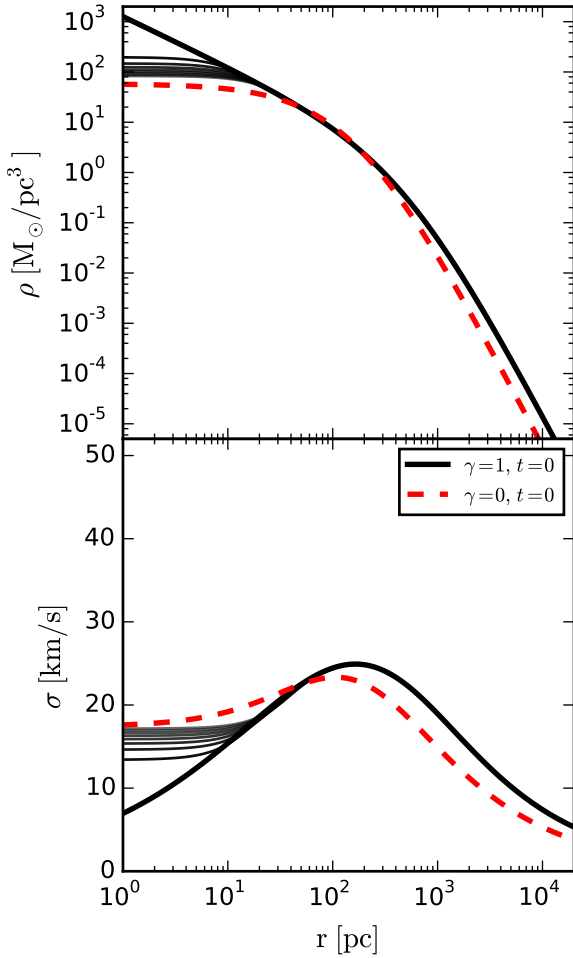


Figure 1. The transition from cusp to core (*top panel*) and the increase of central velocity dispersion (*bottom panel*) due to collisional relaxation effect in a PBH-DM halo. The DM halo has a mass of $2 \times 10^9 M_\odot$ consisting of $30 M_\odot$ PBHs. It has an initial density profile of $\gamma = 1$ and $R_{0,\text{DM}} = 500$ pc, and a central velocity dispersion of 8 km/s, as represented by the thick black curves in both panels. The thin lines show the evolution of the density profile and the projected velocity dispersion from $t = 0$ to 12 Gyr with an interval of 1.5 Gyr. The red dashed lines show the best matching PBH-DM halo of $10^9 M_\odot$ with a core density profile of $\gamma = 0$ and $R_{0,\text{DM}} = 160$ pc, and an increased central velocity dispersion.

DM velocity dispersion peaks at the scale radius. However, if the DM is composed of PBHs, two-body relaxation will soften the central cusp, and as a result of the collisional heating, the velocity dispersion in the central region will increase while the density will drop at the same time. This process leads to the rapid formation of a core (Quinlan 1996) as a result of “temperature inversion”, in which the colder dense cusp will be heated by a hotter envelope.

Figure 1 illustrates how this relaxation effect transforms a PBH-DM halo from a $\gamma = 1$ cusp to a $\gamma = 0$ core. The DM halo has a mass of $2 \times 10^9 M_\odot$ composed of $30 M_\odot$ PBHs, and an initial cuspy density profile of $\gamma = 1$ and $R_{0,\text{DM}} = 500$ pc. Collisional relaxation quickly removes the central density cusp and increases the central velocity dispersion.

After 12 Gyrs, this PBH-DM halo can be approximated by a less massive ($10^9 M_\odot$) one with a core density profile of $\gamma = 0$ and a characteristic scale radius of $R_{0,\text{DM}} = 160$ pc, as shown by the red dashed curves.

In order to determine the time scale of the transition from cusp to core profiles, we set up cuspy DM halos consisting of $30 M_\odot$ PBHs with a total mass in the range from 10^5 to $10^9 M_\odot$ at redshift $z = 10$, based on the mass-concentration relation from Diemer & Kravtsov (2015). We evolve the PBH-DM halos using the FP code PHASEFLOW. These simulations show that the collisional relaxation effect removes the central cusp almost instantaneously, and the DM core grows quickly in size. For instance, it takes only ~ 0.05 Gyr for all the halos to develop a core of ~ 10 pc, and ~ 0.18 Gyr to reach ~ 20 pc. If formed via hierarchical assembly, it would be difficult for DM halos of $10^8 - 10^9 M_\odot$ to retain density cusps in the first place since the central density of their less massive progenitors has already been lowered. We speculate that the density profile of a PBH-DM halo, similar to self-interacting DM (Vogelsberger et al. 2012), could be described by a truncated singular sphere with a sizable core (Shapiro et al. 1999). In the absence of a self-consistent treatment of density profile of PBH-DM halos, we thus use a cored density profile with $\gamma = 0$ for any initial DM scale radius $R_{0,\text{DM}}$ as our default choice for simulations in the following sections. In the Discussion Section, we will include a test using $\gamma = 1$ to examine the outcome with cuspy density profiles.

3.2 Stars in PBH-DM halos

In a system with two components of different masses, two-body encounters and energy exchange would lead to change in the distribution of density and energy. To investigate the evolution of a DM halo with stars and PBHs, we set up a DM halo with a mass of $2 \times 10^9 M_\odot$, which contains $10^3 M_\odot$ of stars, each being $1 M_\odot$, and the DM is composed of $30 M_\odot$ PBHs. The Plummer sphere for the stars has a total mass of $10^3 M_\odot$ and a scale radius of 5 pc, while the Dehnen sphere for the DM has a total mass of $2 \times 10^9 M_\odot$ and a scale radius $R_{0,\text{DM}} = 500$ pc. The system is then followed with the FP code PHASEFLOW, and the results are shown in Figure 2. Due to the huge difference in both mass and size, the two components have different initialization in both density profile and velocity dispersion, and strong two-body relaxation and energy exchange leads to significant change in the stellar density profile and velocity dispersion. Because the PBH is much more massive than the star, heating from PBHs on the stars is the dominant driver for the evolution of the stellar component. After 12 Gyrs, the central stellar density drops by nearly 3 orders of magnitude, as shown in the upper panel of Figure 2, while the central stellar velocity dispersion increases by a factor of ~ 8 , as in the lower panel.

As the density profile of the stars slowly diffuses out, the half-light radius increases. This process depends on the density and velocity dispersion profile of the PBH halo. We note that in Figure 2, the stellar velocity dispersion is well below that of PBH-DM at $t = 12$ Gyr. Hence, equipartition of energy between the two mass species, i.e. $\sigma(m)^2 \propto m^{-1}$, has not been achieved.

As first pointed out by Spitzer (1969), full energy equipartition is possible only if the mass fraction of heavy

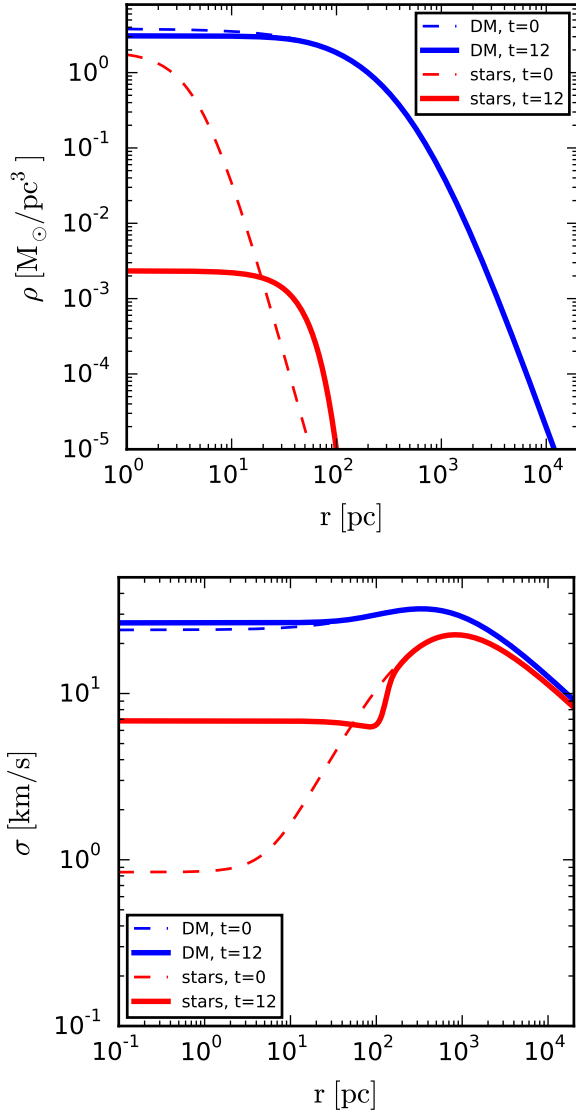


Figure 2. Effects of two-body relaxation and energy exchange on the density profile (*top panel*) and velocity dispersion (*bottom panel*) of a two-component halo system with stars and PBH-DM. The halo has a total DM mass of $2 \times 10^9 M_\odot$ composed of $30 M_\odot$ PBHs, and a total stellar mass of $10^3 M_\odot$ consisting of $1 M_\odot$ stars. The blue curves represent the PBH-DM component at $t = 0$ (dashed lines) and $t = 12$ Gyr (solid lines), while the red curves represent the stellar components at $t = 0$ (dashed lines) and $t = 12$ Gyr (solid lines).

species is below some critical value. In our setup, the total mass ratio between PBHs and stars is well above the critical value $\sim 0.001 (= 0.16(1/30)^{1.5})$. As a result, the central regime will be devoid of stars, leading to only a “partial equipartition”. Recently, [Trenti & van der Marel \(2013\)](#) and [Bianchini et al. \(2016\)](#) reported partial equipartition in their direct N-body simulations of globular clusters. Of course, our example is quite extreme since the mass density profile is completely dominated by PBHs at almost all radii.

The size increase due to heating of PBH appears to be slightly slower than the analytical result obtained by [Brandt](#)

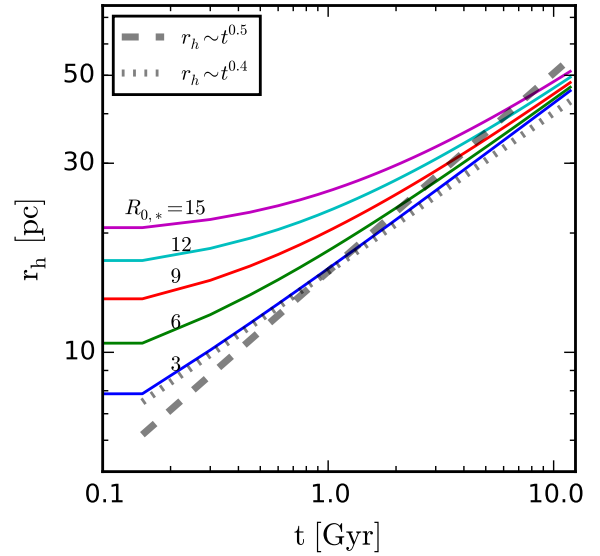


Figure 3. The evolution of 3D half-light radius of stellar components with various initial conditions in a PBH-DM halo from our simulations, in comparison with analytical result from [Brandt \(2016\)](#). The different color represents different initial condition with $R_{0,*}$ varying from 3, 6, 9, 12 and 15 pc, respectively. Our results show a $r_h \sim t^{0.4}$ size growth rate, slower than $r_h \sim t^{0.5}$ reported by [Brandt \(2016\)](#).

(2016). To further investigate this, we performed a set of FP simulations with PHASEFLOW for different initial stellar density distributions, by varying $R_{0,*}$ from 3 to 15 pc, within a fixed Dehnen sphere with a total DM mass of $2 \times 10^9 M_\odot$ and $R_{0,DM} = 500$ pc. The resulting size evolution of the different stellar components is shown in Figure 3, in comparison with that of [Brandt \(2016\)](#). Our simulations show a slower growth rate, $r_h \propto t^{0.4}$, than that of $r_h \propto t^{0.5}$ by [Brandt \(2016\)](#). The heating rate of a less concentrated stellar component is also slower than those of more concentrated ones. For example, the magenta line on top of Figure 3 shows the size evolution of a stellar core from $R_{0,*} = 15$ pc, which only approaches the asymptotic $t^{0.4}$ trend by the end of the integration. Our results suggest that the final size of the stellar core only depends weakly on the initial size, and that after ~ 10 Gyrs, a two-component PBH-DM halo of $2 \times 10^9 M_\odot$ would produce a stellar core of ~ 50 pc regardless of its initial size.

From Figure 2, the stellar density profile after $t = 12$ Gyrs is very smooth, we do not see any “ring profile” predicted by [Koushiappas & Loeb \(2017\)](#). The discrepancy may be due to the different methods used to track the evolution of the halo system. The FP simulations we performed with PHASEFLOW can track the two-body relaxation and energy exchange between the different mass components accurately, while the analytical formula used by [Koushiappas & Loeb \(2017\)](#) may not be able to follow the evolution of the system dynamically.

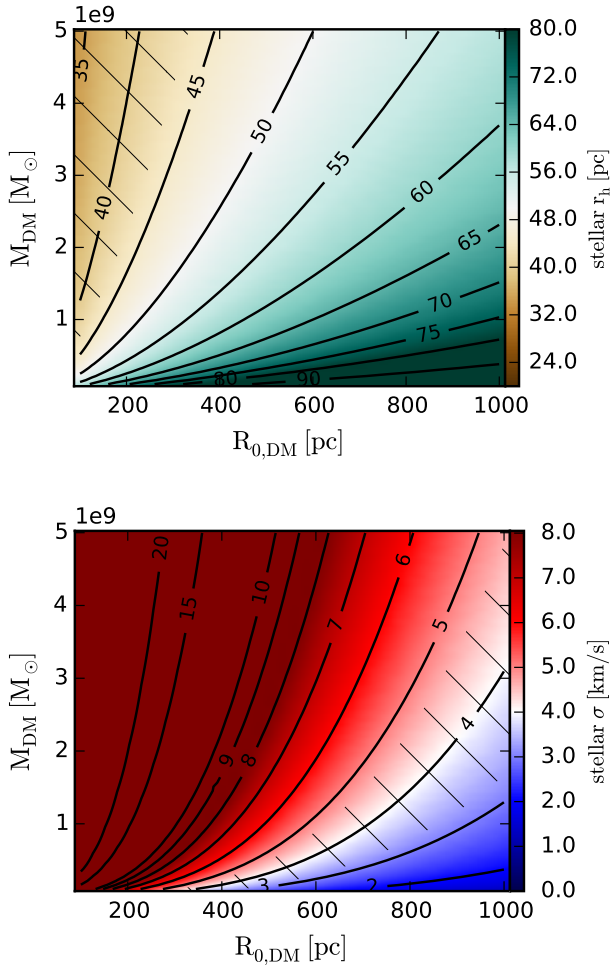


Figure 4. The distribution of 3D half-mass radius (*top panel*) and projected velocity dispersion (*bottom panel*) of the stellar components in the PBH-DM halo parameter space, from 2500 FP simulations using the PHASEFLOW code. There are 50 grids for each of the DM halo parameters, total DM mass M_{DM} and scale radius $R_{0,\text{DM}}$. The DM is assumed to consist of PBHs of $30 M_{\odot}$. The allowed regions by observations are highlighted and hatched in both panels which, however, have little overlap with each other.

3.3 Parameter space of PBH-DM halos from FP simulations

In order to explore the parameter space of DM halos of the observed compact ultra-faint dwarfs in Table 1, we use the FP code PHASEFLOW to perform a grid of dynamical simulations of the two-component systems consisting of stars and PBH-DM with different halo mass and size. We vary the total DM mass from 10^8 to $5 \times 10^9 M_{\odot}$, and vary the scale radius of the DM Dehnen sphere from 100 pc to 1000 pc. We consider 50 values for each of the two DM halo parameters, M_{DM} and $R_{0,\text{DM}}$, resulting in a total of 2500 simulations. We assume the DM is composed of PBHs of $30 M_{\odot}$, a total stellar mass of $10^3 M_{\odot}$, and an initial stellar scale radius of $R_{0,*} = 20$ pc. Each system is integrated for a duration of 12 Gyrs.

The final half-mass radius and the projected central ve-

locity dispersion of the stars are shown in Figure 4, as functions of the DM parameter space of total DM masses M_{DM} and scale radius $R_{0,\text{DM}}$. The shaded regions in both the top and bottom panels indicate the allowed range of DM parameters from the observations of the compact ultra-faint dwarfs. From the stellar half-mass radius distribution in the *top panel*, given the same total DM mass, the spreading of the stellar component is more efficient when the scale radius is larger. While with the same scale radius, less massive halos show more efficient heating. When the halo is less dense (either due to larger scale radius or lower mass), the initial velocity dispersions of both stars and PBHs are also much lower. In this case, the relative increase of stellar velocity dispersion is larger than in a more dense halo. The preferred range of $r_h \sim 25 - 40$ pc from observations demand a narrow range of $R_{0,\text{DM}} < 400$ pc and $M_{\text{DM}} < 5 \times 10^9 M_{\odot}$. On the other hand, from the stellar velocity dispersion in the *bottom panel*, the preferred range of $\sigma \sim 3 - 5$ km/s dictates a range of $300 < R_{0,\text{DM}} < 1000$ pc and $M_{\text{DM}} > 10^9 M_{\odot}$.

Clearly, it is difficult to reconcile the two constraints simultaneously. A smaller stellar size would require a DM halo with smaller scale radius, thus reducing the heating from relaxation by increasing the velocity dispersion. Given PBH mass of $30 M_{\odot}$ and a typical size of ~ 40 pc (de-projected), there is little room in the plane of M_{DM} and $r_{0,\text{DM}}$ to meet both the constraints.

3.4 MCMC constraints on PBH-DM from compact ultra-faint dwarfs

In order to constrain the PBH-DM parameters from observations, we use the stellar half-mass radius and stellar velocity dispersion of the observed compact ultra-faint dwarfs in Table 1 as priors and perform a total of 10^5 MCMC realizations using the EMCEE code. The resulting posterior probability distributions of the four model parameters, the DM scale radius $R_{0,\text{DM}}$, initial stellar component scale radius $R_{0,*}$, total DM mass M_{DM} , and PBH mass M_{BH} , are shown in Figure 5, respectively.

The posterior surface in the plane of $R_{0,\text{DM}}$ and $M_{0,\text{DM}}$ can be understood with the help of Figure 4, as a balance between the requirements of small sizes and small velocity dispersions. The contours in the plane of $R_{0,\text{DM}}$ and $M_{0,\text{DM}}$ roughly covers a narrow region of constant DM density defined by $M_{\text{DM}} \propto R_{0,\text{DM}}^3$.

Moreover, the likelihood distribution of the initial stellar size $R_{0,*}$ and M_{BH} has two major features, which correspond to two major class of allowed configurations. First, there is a vertical region with $\log(R_{0,*})$ close to the average size of the observed dwarfs with $\log(M_{\text{BH}})$ close to 0. This is a class of models with little heating and, hence, insignificant size evolution for the stars. Second, there is a horizontal band where $\log(M_{\text{BH}})$ is close to 1 and $\log(R_{0,*})$ close to 1. This is the allowed parameter space where a substantial heating by PBHs expands the initially more compact stellar distribution up to its present size.

From these distributions, the most probable results of the four parameters are listed in Table 2: $\log(R_{0,\text{DM}}/\text{pc}) = 2.77$, $\log(R_{0,*}/\text{pc}) = 1.47$, $\log(M_{\text{DM}}/M_{\odot}) = 9.12$, and $\log(M_{\text{BH}}/M_{\odot}) = 0.93$. Note these results are similar to those obtained from simulations assuming cuspy initial DM density profiles, as shown in the table and discussed in § 4.

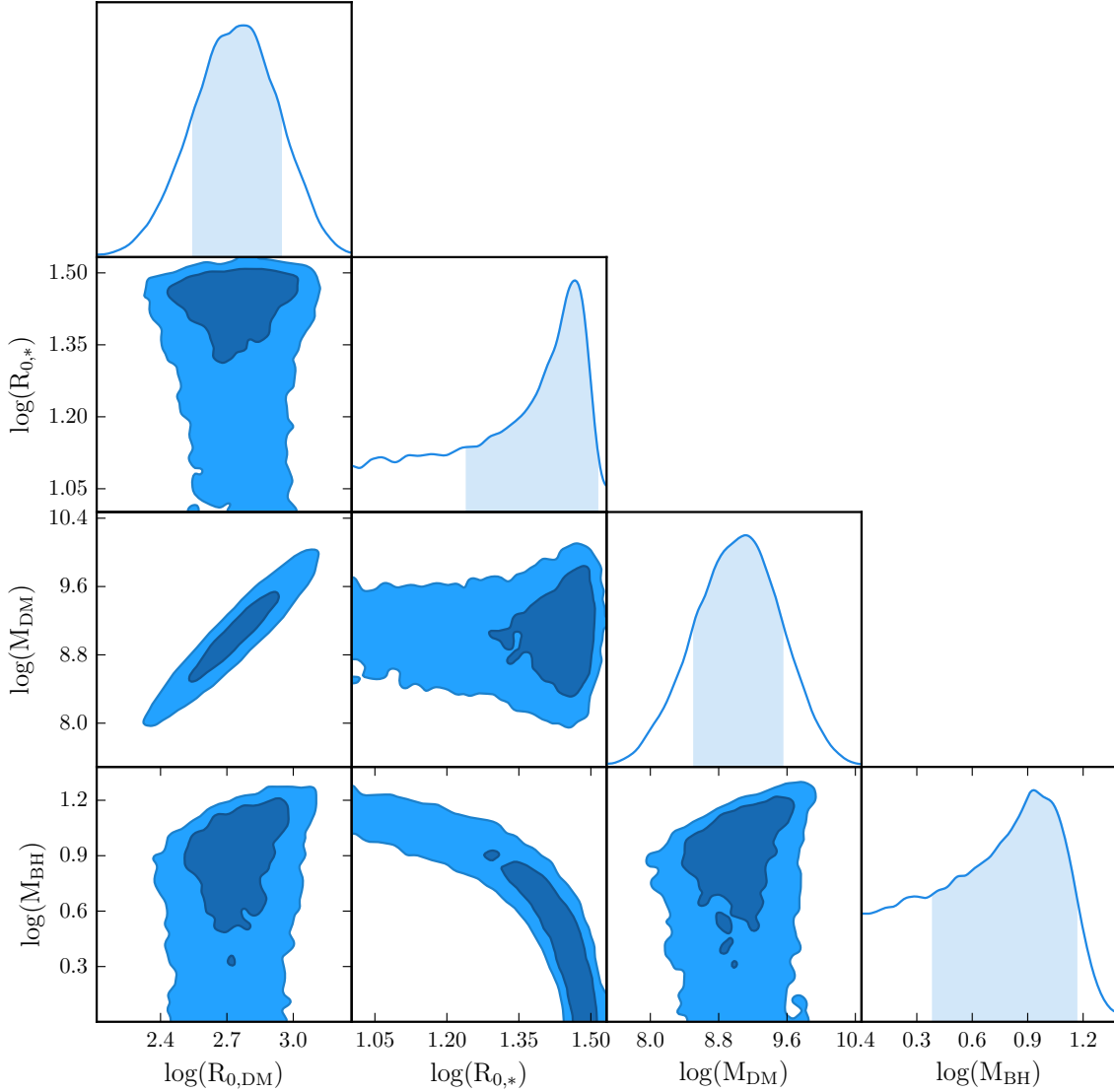


Figure 5. Posterior probability distributions of the four PBH-DM parameters constrained by the stellar half-mass radius and stellar velocity dispersion of observed compact ultra-faint dwarfs: the DM scale radius $R_{0,DM}$, initial stellar component scale radius $R_{0,*}$, total DM mass M_{DM} , and PBH mass M_{BH} . The contours indicate the 1- and 2- σ uncertainty region. This plot is generated using the Python package ChainConsumer (Hinton 2016).

Our results indicate that these galaxies must be DM-dominated: the posterior distribution of the central DM density lies in a narrow range of $1\text{--}2\text{ M}_{\odot}/\text{pc}^3$ while the stellar density is two orders of magnitude lower. We also experimented with models having no DM component at all. In this case, the velocity dispersion of stars would be much lower than the observed value for the given combination of total stellar mass and half-mass radius. By contrast, globular clusters have a far larger stellar mass while occupying the same region in the $R_{*}\text{--}\sigma$ plane. The existence of DM also ensures the logic of using ultra-faint dwarf galaxies to constrain PBH mass is self-consistent.

The constraint on PBH mass in the massive end comes from a maximum heating rate, which is more stringent than that from the lower-mass end, mainly due to the assumptions upon which the stellar component was initialized, as we discuss in § 4. This can also be seen in the contour of $R_{*,0}$

and $\log(M_{BH})$, which is a continuous distribution. Models with $R_{*,0}$ between 20 and 30 pc are certainly allowed, with a modest heating from PBH that brings the stellar size and velocity dispersion close to the observed values. Note that the peak of M_{BH} does not correspond to the peak of $R_{*,0}$. Therefore, the likelihood surface in the plane of $R_{0,*}$ and M_{BH} is more informative, and the constraints on M_{BH} is limited by our prior knowledge of $R_{0,*}$.

The estimate can be improved if we have better prior information about the initial size of the stellar component. There is a clear dichotomy in the spread in metallicity between dwarf galaxies and globular clusters of the same luminosities (see Willman & Strader 2012, most of the observed globular clusters show < 0.1 dex metallicity spread). The large metallicity spread (> 0.2 dex) among the member stars in the dwarf galaxies could impose more stringent constraints on the initial stellar component size. Gas con-

Table 2. Results from 10^5 MCMC realizations assuming cored and cuspy DM density profiles

model	$\log(R_{0,\text{DM}})$	$\log(R_{0,*})$	$\log(M_{\text{DM}})$	$\log(M_{\text{BH}})$
core	$2.77^{+0.17}_{-0.22}$	$1.47^{+0.05}_{-0.23}$	$9.12^{+0.42}_{-0.61}$	$0.93^{+0.23}_{-0.54}$
cuspy	$3.34^{+0.26}_{-0.28}$	$1.46^{+0.05}_{-0.27}$	$8.92^{+0.55}_{-0.44}$	$0.78^{+0.11}_{-0.41}$

finer in a small volume would lead to efficient mixing due to multiple supernova events, hence a more uniform metallicity distribution is incompatible with observations. If the initial size $R_{0,*}$ is above 20 pc, then M_{BH} would fall below $10 M_{\odot}$.

4 DISCUSSIONS

4.1 Model uncertainties

In our models, the strongest prior is the total DM halo mass, which fulfills the requirement that these halos should be just slightly more massive than the minimum mass required for star formation. For the other three free parameters, we have adopted rather agnostic prior distributions. The initial distribution of stellar component, which follows a Plummer sphere, is a reasonable assumption.

Our model assumes that DM halo has a density core. This is a reasonable assumption given that the collisional effect on a cusped density profile is well understood. To demonstrate this, we have run another set of MCMC realizations with a density cusp ($\gamma = 1$) at $t = 0$. As shown in Figure 6, the final distributions of the four parameters are close to those in Figure 5, although the peak of $\log(M_{\text{BH}})$ drops slightly from 0.93 to 0.78. This is due to extra heating as the central velocity dispersion is low for a cuspy density profile. A comparison of the marginalized posterior distributions for both cored and cuspy profiles is given in Table 2.

Our choice of prior distribution of total DM mass also a reasonable one. As illustrated in Figure 5, the total DM halo mass M_{DM} does not have strong correlation with either M_{BH} or $R_{*,0}$. The covariance between M_{DM} and $R_{0,\text{DM}}$ covers a region defined by a constant DM density in the range of $1\text{--}2 M_{\odot}/\text{pc}^3$. In contrast, PBH mass is strongly correlated with the initial size of the stellar component. Therefore, our constraints on PBH mass is unaffected by the prior distribution of total DM mass. Moreover, if more compact ultra-faint dwarfs are to be discovered in the near future, their cumulative number could impose yet another constraint against the possibility of massive M_{\odot} PBHs as DM.

There are several limitations in our approach need to be stressed. First, we treat the halos in isolation while in reality they are in highly tumultuous galactic environments, subjected to various mass loss processes (Zhu et al. 2016). Second, we use the measurements of the compact ultra-faint dwarfs as an input for the likelihood function and treat the reported uncertainties as the widths of Gaussians in the likelihood function. We have used a smaller half-mass size for Ret II and Hor I between those reported by Koposov et al. (2015) and Bechtol et al. (2015). Accurate determination of the membership of stars in such faint galaxies is an extremely challenging task. In addition, unresolved binary stars may significantly inflate the observed velocity dispersion in these cold systems, although they are unlikely to completely dominate the measurements (McConnachie & Côté 2010). Should

the true size of these stellar systems change, our modeling and conclusions need to be revisited accordingly.

In our model, there is a built-in bias which puts more emphasis on the more massive PBH for the following reason. If the collisional relaxation effect is negligible, only a limited region around $r_h = 40$ pc and $\sigma = 4$ km/s is allowed. On the other hand, if the model starts with a smaller initial size (with a smaller velocity dispersion), a modest heating will bring both the size and the velocity dispersion closer to the observed values. Therefore, *some* heating effect can be slightly more favored than *no* heating effect if there are more models with modest heating allowed than those with little heating.

4.2 Comparison with previous works

We believe that our analysis improves upon the previous calculations by Brandt (2016) and Koushiappas & Loeb (2017) by using a FP code and an MCMC approach. In particular, the FP code self-consistently evolved the two components system with two mass species. In the latter study, the velocity dispersion profiles of the two components are assumed to be the same, while our modeling clearly shows this is not the case using the FP code.

Moreover, our calculations show that the heating rate from the massive species on the light species is slightly less efficient than $t^{0.5}$, a result of partial equipartition of energy due to the dominant contribution from PBHs. In addition, the combination of the FP code and a MCMC approach is able to utilize both size and kinematics of the observed ultra-compact dwarf galaxies by efficiently sampling the parameter space.

We note that the stellar density profile by the end of the integration always contains a “diffused” core in our FP calculation. This is not the same as the ring profile predicted by Koushiappas & Loeb (2017). The main reason for this discrepancy is that the size evolution formula used by Koushiappas & Loeb (2017) may not be accurately applicable at all radii. On the other hand, the spreading out of the surface density profiles are very similar to Koushiappas & Loeb (2017).

Our model assumes that the DM is completely composed of PBHs. It was suggested by Brandt (2016) that PBH above $10 M_{\odot}$ may be firmly excluded as the primary candidate of DM in dwarf galaxies. The constraint from Koushiappas & Loeb (2017) is slightly stronger, with masses greater than $6 M_{\odot}$ excluded. The constraint derived from our analysis is slightly less restrictive compared to these two studies.

4.3 Observational signatures of PBHs with millisecond time delay

Our analysis is consistent with the suggestion that PBHs in the mass range of $25\text{--}100 M_{\odot}$ are ruled out as the main component of DM (Brandt 2016; Carr et al. 2017). If the LIGO detections are from mergers of PBH binaries of $\sim 30 M_{\odot}$, it is only possible if they are in the massive tail of an extended PBH mass function (Magee & Hanna 2017). However, any PBHs with a mass substantially higher than $10 M_{\odot}$ would violate the constraints from the dynamical analysis of dwarf galaxies. In the near future, aLIGO observations may soon provide constraints on PBHs around $10 M_{\odot}$.

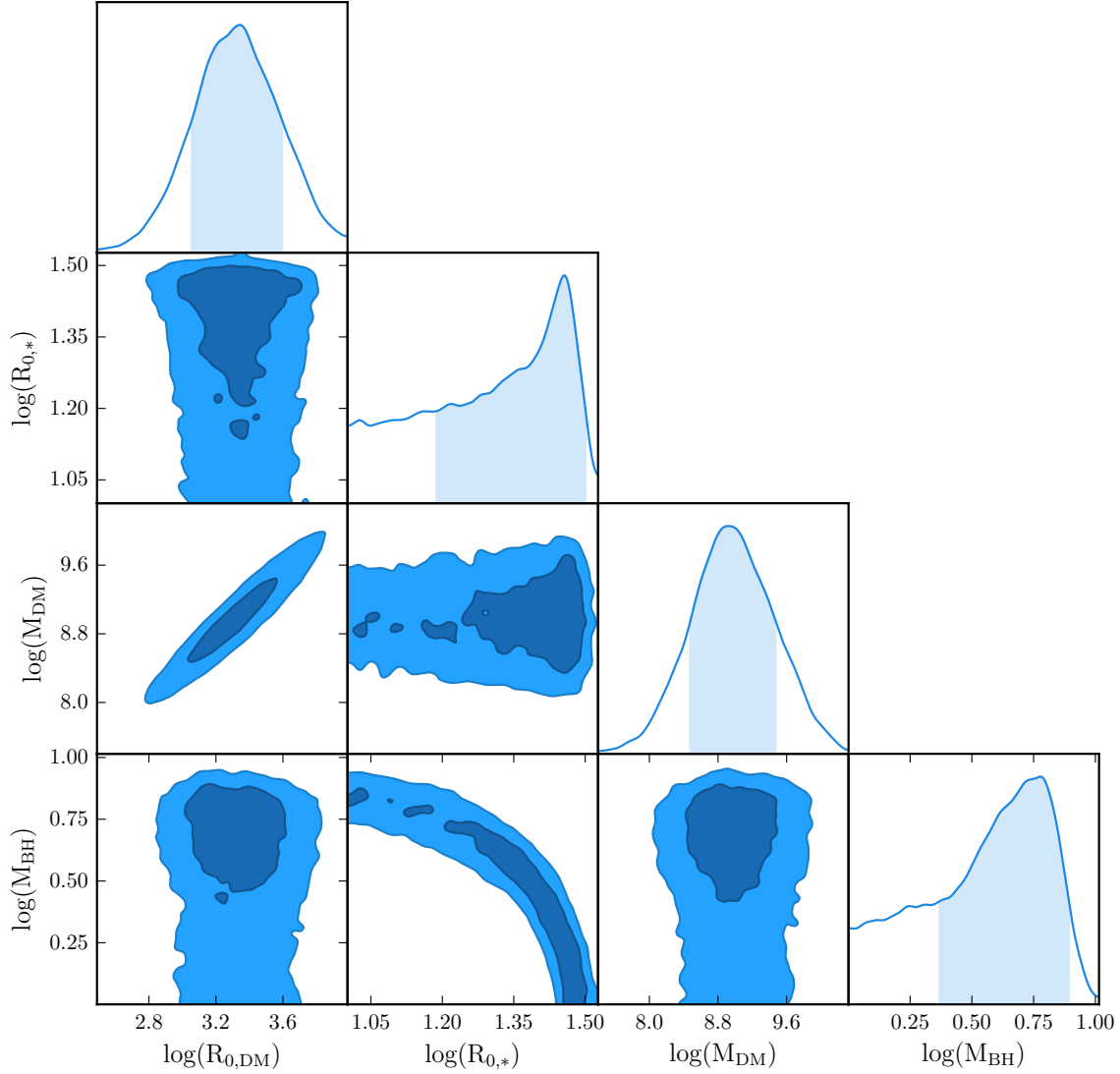


Figure 6. Same as Figure 5, but for a Dehnen halo with a cusp ($\gamma = 1$) at $t = 0$. The prior distribution of $\log(R_{0,DM})$ is rescaled to $\sim \mathcal{U}(\log(200), \log(10000))$ in order to cover the allowed PBH halo parameter space.

It remains possible that *some* fraction of the DM may be PBHs in this mass range. Apart from the contribution to the total DM budget, the existence of PBHs will provide important constraints on certain inflation theories. In addition, gravitational lensing due to $\sim 10 M_{\odot}$ PBHs will induce a time delay on the order of milliseconds (Mao 1992; Muñoz et al. 2016). There are at least two known astrophysical phenomena that can produce detectable signals on this rapid time scale. One is fast radio burst (Lorimer et al. 2007). If fast radio bursts have indeed cosmological origin (Spitler et al. 2016), then one would expect repeated bursts with millisecond delay from the same location of the sky within a large number (Fialkov & Loeb 2017) of bursts due to the PBH lenses (Muñoz et al. 2016).

Another promising source in the kHz regime for the detection of PBHs would be gravitational waves from stellar mass BH mergers. Similar to the mechanism of femtolensing of γ -ray burst (Gould 1992), millisecond delays could induce a characteristic interference pattern in the detected

waveforms in the merger phase due to the interference of two lensed images.

Perhaps gravitational waves are better sources than radio bursts since they do not suffer from interstellar dispersions. This technique could be feasible with the next generation detectors such as the “Cosmic Explorer” (Abbott et al. 2017). With a large number of gravitational wave detections, we could place a strong constraint on the mass fraction of PBHs in Ω_M , since the lensing optical depth is at the same order as the mass fraction of PBHs for cosmological sources (Press & Gunn 1973).

5 SUMMARY

In this study, we improve the recent analytical work of Brandt (2016) and Koushiappas & Loeb (2017) on the investigation of the possibility of DM consisting entirely of PBHs, by combining Fokker–Planck simulations with Markov Chain Monte Carlo realizations. The former

method, implemented in the code PHAEFLOW, accurately follows the joint evolution of stars and PBH-DM driven by two-body relaxation, for a given choice of parameters. By combining it with the MCMC approach, we explore the parameter space and use the half-light radius and central stellar velocity dispersions of observed compact ultra-faint dwarf galaxies as joint priors in the MCMC sampling to constrain the PBH-DM parameters. Our findings can be summarized as follows:

- For a DM halo in the mass range of $10^6 - 10^9 M_\odot$, if the DM is composed of PBHs entirely, collisional relaxation quickly transforms a cusp to a cored density profile.
- For a system with stars and PBH-DM, two-body relaxation between the stars and PBH-DM drives up the stellar core size, and heating from the PBHs increases the central stellar velocity dispersion. The size evolution of the stellar core has a growth rate of $r_h \propto t^{0.4}$, which is slightly slower than that from the full energy equipartition ($r_h \propto t^{0.5}$).
- The joint constraints from the observed half-light radius and central stellar velocity dispersions of compact ultra-faint dwarf galaxies leave a narrow parameter space of DM halos consist of PBHs. Results from the MCMC simulations suggest that the central density of DM halo has a narrow range of $1-2 M_\odot/\text{pc}^3$, and the mass of PBHs is most likely within $2-14 M_\odot$, if the DM is completely made of PBH.

We note that our constraint of PBHs is slightly less restrictive than those of Brandt (2016) and Koushiappas & Loeb (2017). Although PBH with mass above $10 M_\odot$ can be excluded as the primary candidate of DM from our results, we emphasize that our models are inconclusive, and that the nature of DM remains elusive.

ACKNOWLEDGEMENTS

It is our great pleasure to thank Avi Loeb, Lars Hernquist, Savvas Koushiappas and Peter Mészáros for stimulating discussions. YL acknowledges support from NSF grants AST-0965694, AST-1009867, AST-1412719, and MRI-1626251. The numerical computations and data analysis in this paper have been carried out on the CyberLAMP cluster supported by MRI-1626251, operated and maintained by the Institute for CyberScience at the Pennsylvania State University, as well as the Odyssey cluster supported by the FAS Division of Science, Research Computing Group at Harvard University. The Institute for Gravitation and the Cosmos is supported by the Eberly College of Science and the Office of the Senior Vice President for Research at the Pennsylvania State University. EV acknowledges support from the European Research Council under the 7th Framework Programme (grant 321067).

REFERENCES

Abbott B. P., et al., 2017, *Classical and Quantum Gravity*, **34**, 044001
 Afshordi N., McDonald P., Spergel D. N., 2003, *ApJ*, **594**, L71
 Amorisco N. C., 2017, preprint, ([arXiv:1704.06262](https://arxiv.org/abs/1704.06262))

Bechtol K., et al., 2015, *ApJ*, **807**, 50
 Bianchini P., van de Ven G., Norris M. A., Schinnerer E., Varri A. L., 2016, *MNRAS*, **458**, 3644
 Binney J., Tremaine S., 2008, *Galactic Dynamics: Second Edition*. Princeton University Press
 Bird S., Cholis I., Muñoz J. B., Ali-Haïmoud Y., Kamionkowski M., Kovetz E. D., Raccanelli A., Riess A. G., 2016, *Physical Review Letters*, **116**, 201301
 Brandt T. D., 2016, *ApJ*, **824**, L31
 Carr B. J., Hawking S. W., 1974, *MNRAS*, **168**, 399
 Carr B., Kühnel F., Sandstad M., 2016, *Phys. Rev. D*, **94**, 083504
 Carr B., Raidal M., Tenkanen T., Vaskonen V., Veermäe H., 2017, *Phys. Rev. D*, **96**, 023514
 Chan T. K., Kereš D., Oñorbe J., Hopkins P. F., Muratov A. L., Faucher-Giguère C.-A., Quataert E., 2015, *MNRAS*, **454**, 2981
 Contenta F., et al., 2017, preprint, ([arXiv:1705.01820](https://arxiv.org/abs/1705.01820))
 Dehnen W., 1993, *MNRAS*, **265**, 250
 Di Cintio A., Brook C. B., Dutton A. A., Macciò A. V., Stinson G. S., Knebe A., 2014, *MNRAS*, **441**, 2986
 Diemer B., Kravtsov A. V., 2015, *ApJ*, **799**, 108
 Fialkov A., Loeb A., 2017, *ApJ*, **846**, L27
 Foreman-Mackey D., Hogg D. W., Lang D., Goodman J., 2013, *PASP*, **125**, 306
 Frampton P. H., Kawasaki M., Takahashi F., Yanagida T. T., 2010, *J. Cosmology Astropart. Phys.*, **4**, 023
 Garrison-Kimmel S., Bullock J. S., Boylan-Kolchin M., Bardwell E., 2017, *MNRAS*, **464**, 3108
 Gnedin N. Y., Kaurov A. A., 2014, *ApJ*, **793**, 30
 Gould A., 1992, *ApJ*, **386**, L5
 Hawking S., 1971, *MNRAS*, **152**, 75
 Hernquist L., 1990, *ApJ*, **356**, 359
 Hinton S., 2016, *JOSS*, **1**
 Hirano S., Sullivan J. M., Bromm V., 2017, preprint, ([arXiv:1706.00435](https://arxiv.org/abs/1706.00435))
 Hu W., Barkana R., Gruzinov A., 2000, *Physical Review Letters*, **85**, 1158
 Hui L., Ostriker J. P., Tremaine S., Witten E., 2017, *Phys. Rev. D*, **95**, 043541
 Koposov S. E., Belokurov V., Torrealba G., Evans N. W., 2015, *ApJ*, **805**, 130
 Koushiappas S. M., Loeb A., 2017, *Phys. Rev. Lett.*, **119**, 041102
 Lorimer D. R., Bailes M., McLaughlin M. A., Narkevic D. J., Crawford F., 2007, *Science*, **318**, 777
 Ma X., et al., 2017, preprint, ([arXiv:1706.06605](https://arxiv.org/abs/1706.06605))
 Magee R., Hanna C., 2017, preprint, ([arXiv:1706.04947](https://arxiv.org/abs/1706.04947))
 Mao S., 1992, *ApJ*, **389**, L41
 McConnachie A. W., Côté P., 2010, *ApJ*, **722**, L209
 Meszaros P., 1975, *A&A*, **38**, 5
 Muñoz J. B., Kovetz E. D., Dai L., Kamionkowski M., 2016, *Physical Review Letters*, **117**, 091301
 Navarro J. F., Frenk C. S., White S. D. M., 1997, *ApJ*, **490**, 493
 Okamoto T., Gao L., Theuns T., 2008, *MNRAS*, **390**, 920
 Plummer H. C., 1911, *MNRAS*, **71**, 460
 Pontzen A., Governato F., 2014, *Nature*, **506**, 171
 Press W. H., Gunn J. E., 1973, *ApJ*, **185**, 397
 Quinlan G. D., 1996, *New Astron.*, **1**, 255
 Read J. I., Agertz O., Collins M. L. M., 2016, *MNRAS*, **459**, 2573
 Sawala T., et al., 2015, *MNRAS*, **448**, 2941
 Shapiro P. R., Iliev I. T., Raga A. C., 1999, *MNRAS*, **307**, 203
 Spitler L. G., et al., 2016, *Nature*, **531**, 202
 Spitzer Jr. L., 1969, *ApJ*, **158**, L139
 The LIGO Scientific Collaboration et al., 2016a, *Physical Review Letters*, **116**, 061102
 The LIGO Scientific Collaboration et al., 2016b, *Physical Review Letters*, **116**, 241103
 The LIGO Scientific Collaboration et al., 2017a, preprint, ([arXiv:1709.09660](https://arxiv.org/abs/1709.09660))

- The LIGO Scientific Collaboration et al., 2017b, [Physical Review Letters](#), **118**, 221101
- Trenti M., van der Marel R., 2013, [MNRAS](#), **435**, 3272
- Vasiliev E., 2017, [ApJ](#), **848**, 10
- Vogelsberger M., Zavala J., Loeb A., 2012, [MNRAS](#), **423**, 3740
- Vogelsberger M., Zavala J., Cyr-Racine F.-Y., Pfrommer C., Bringmann T., Sigurdson K., 2016, [MNRAS](#), **460**, 1399
- Weinberg D. H., Bullock J. S., Governato F., Kuzio de Naray R., Peter A. H. G., 2015, [Proceedings of the National Academy of Science](#), **112**, 12249
- Wheeler C., Oñorbe J., Bullock J. S., Boylan-Kolchin M., Elbert O. D., Garrison-Kimmel S., Hopkins P. F., Kereš D., 2015, [MNRAS](#), **453**, 1305
- Willman B., Strader J., 2012, [AJ](#), **144**, 76
- Wolf J., Martinez G. D., Bullock J. S., Kaplinghat M., Geha M., Muñoz R. R., Simon J. D., Avedo F. F., 2010, [MNRAS](#), **406**, 1220
- Yoshida N., Sokasian A., Hernquist L., Springel V., 2003, [ApJ](#), **591**, L1
- Zhao H., 1996, [MNRAS](#), **278**, 488
- Zhu Q., Marinacci F., Maji M., Li Y., Springel V., Hernquist L., 2016, [MNRAS](#), **458**, 1559

This paper has been typeset from a \LaTeX file prepared by the author.